Deep Contactless Fingerprint Unwarping

Ali Dabouei, Sobhan Soleymani, Jeremy Dawson, Nasser M. Nasrabadi
West Virginia University
{ad0046, ssoleyma}@mix.wvu.edu, {jeremy.dawson, nasser.nasrabadi}@mail.wvu.edu

Abstract

Contactless fingerprints have emerged as a convenient, inexpensive, and hygienic way of capturing fingerprint samples. However, cross-matching contactless fingerprints to the legacy contact-based fingerprints is a challenging task due to the elastic and perspective distortion between the two modalities. Current cross-matching methods merely rectify the elastic distortion of the contact-based samples to reduce the geometric mismatch and ignore the perspective distortion of contactless fingerprints. Adopting classical deformation correction techniques to compensate for the perspective distortion requires a large number of minutiae-annotated contactless fingerprints. However, annotating minutiae of contactless samples is a labor-intensive and inaccurate task especially for regions which are severely distorted by the perspective projection. In this study, we propose a deep model to rectify the perspective distortion of contactless fingerprints by combining a rectification and a ridge enhancement network. The ridge enhancement network provides indirect supervision for training the rectification network and removes the need for the ground truth values of the estimated warp parameters. Comprehensive experiments using two public datasets of contactless fingerprints show that the proposed unwarping approach, on average, results in a 17% *increase in the number of detectable minutiae from contactless fingerprints. Consequently, the proposed model achieves the equal error rate of 7.71% and Rank-1 accuracy of 61.01% on the challenging dataset of '2D/3D' fingerprints.*

1. Introduction

During the past two decades, the ubiquitous adoption of fingerprint-based identification methods have indicated the dominance of fingerprints over other biometric modalities. The random nature of the type and location of features, especially minutiae, in a fingerprint provides reliable and highly discriminative information for fingerprint identification tasks. Ideally, the number of these features within a single fingerprint is large enough that even a partial latent fingerprint collected from a crime scene may be used to identify an individual [4, 8]. Capturing fingerprints is fast, easy, and relatively inexpensive. The convenience of capturing fingerprints has further been improved by utilizing contactless fingerprint devices and developing appropriate recognition techniques. These methods are adopted for either dedicated capturing hardware [1, 15] or existing devices such as mobile phones [26, 27, 23]. Using ordinary cameras to capture contactless fingerprint samples has drawn increasing attention in recent years due to two main factors. First, it is cheaper to employ an existing host device, such as a cell phone, to capture samples. Second, the contactless fingerprint recognition algorithm can be incorporated as an authentication unit on the host device itself.

Despite the many benefits of contactless fingerprint recognition systems, identifying the contactless fingerprints is a challenging problem. In an unconstrained scenario, a finger can be under non-ideal and varying environmental conditions, such as nonuniform illumination. These conditions often reduce the performance of classical ridge enhancement and minutiae extraction methods [11]. Therefore, some algorithms require constraints on the image capture process in order to mitigate the effects of environmental variations [15]. However, these capture constraints can critically limit the application space of the recognition system. In addition to environmental variations, the perspective distortion introduced by the 3D geometry of the finger makes it more difficult to extract information from a contactless fingerprint image using classical algorithms. For instance, perspective distortion severely alters the range of the ridge frequencies. Consequently, classical ridge enhancement methods fail to reconstruct the whole ridge map since they consider a smooth ridge frequency map with a small change around the fingerprint area [11].

As the amount of perspective distortion increases at a distance away from the center of the finger in the contactless fingerprint, several studies suggest considering solely the central region of the fingerprint for the matching process [17, 19]. However, limiting the processing area within a fin-

978-1-7281-3640-0/19/$31.00 ©2019 IEEE

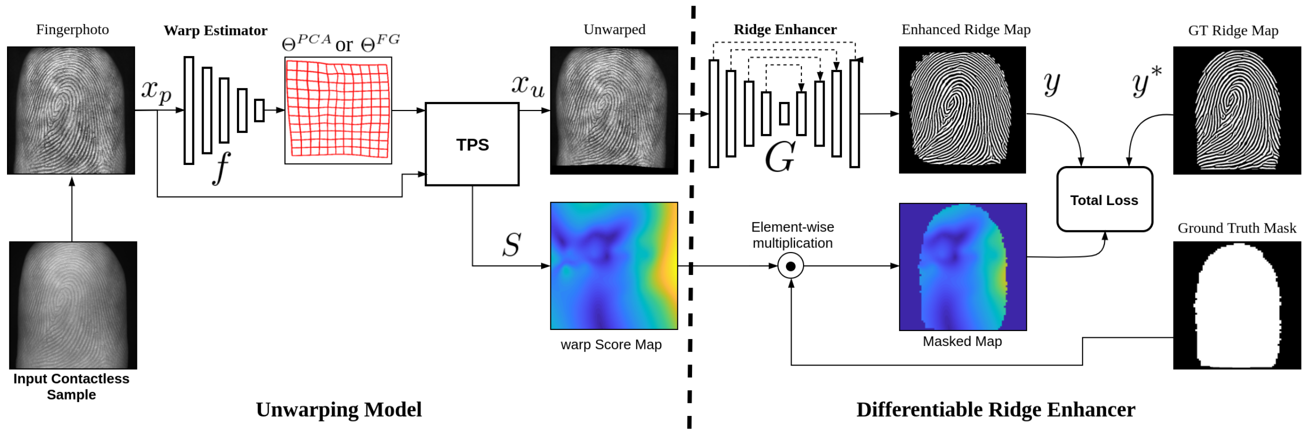

Figure 1. Complete diagram of the model. After preprocessing the input contactless sample, the first network called the warp estimator predicts the parameters of the warp. It can predict the deformation based on either the PCA-constrained (Sec. 2.1.1) or the free grid (Sec. 2.1.2) model of warp. Using the estimated warp parameters, we unwarp the contactless sample. The second network, performs ridge segmentation on the unwarped sample to produce an equivalent binarized ridge map of the ground truth contact-based fingerprint. The final output of the model is then compared to the ground truth ridge map to provide the supervision (Sec. 2.3) needed for updating the parameters of the ridge enhancer and the warp estimator.

gerprint reduces the number of minutiae and may decrease the matching accuracy [12, 6]. An alternative approach is to utilize the localized texture patterns called *level zero* features from the whole contactless fingerprint which can be extracted either directly [14, 23], or indirectly [16, 18] by training a deep convolutional neural network (CNN). The main limitation of these methods is the constrained interoperability of the algorithm since they cannot provide a semantic representation for a given contactless fingerprint that can be matched against fingerprint samples from various contact-based devices. Rectifying the perspective distortion of the contactless fingerprints can increase the active area for the matching process and, consequently, can result in a higher matching accuracy. On the other hand, the rectified contactless fingerprint can represent a 'clean' sample of a finger that is compatible for matching to the legacy samples by extracting reliable minutiae. Several approaches have been proposed in the literature to address the elastic deformation of fingerprints introduced during the capturing process [24, 21, 22, 25, 7, 17]. Thin Plate Spline (TPS) and its approximation [3] have been widely adopted to rectify the elastic distortion of fingerprints [2, 25, 17, 7].

As previously discussed, perspective distortion can prevent the classical fingerprint enhancement algorithms from extracting reliable ridge information from areas which are far from the center of the contactless sample. Therefore, there is not enough supervision (ground truth parameters of the perspective distortion) to directly train a model to predict the parameters of the warp. In this study, we develop a deep contactless fingerprint unwarping model that learns to estimate the distortion parameters of the contactless fingerprints without requiring a direct access to the ground truth distortion parameters. Our model consists of two jointly optimized networks as shown in Figure 1. The first network estimates the warp parameters that can geometrically map the input contactless fingerprint to its equivalent contact-based sample. The second network enhances the unwarped sample to extract the binarized ridge map of the corresponding contact-based fingerprint. We propose a joint optimization framework to couple the two networks and indirectly learns the geometric mapping between the contactless fingerprint and its equivalent contact-based fingerprint. In summary, the contributions of the paper are as follows:

- A novel deep unwarping model is proposed to rectify the perspective distortion of a contactless fingerprint, such that the binarized ridge map of the unwarped contactless fingerprint matches the ridge map of its corresponding contact-based fingerprint.
- An end-to-end joint optimization framework is proposed to solve the problem in a weakly supervised manner, *i.e.*, there is no need for the ground truth parameters of the distortion.
- A differentiable ridge enhancer model is developed to reduce the environmental variations of contactless fingerprints and provide an indirect supervision for the unwarping model.
- A novel statistical model of the perspective warp is developed which provides a more robust representation of the warp compared to conventional PCA-based models.

2. Methods

As discussed in Section 1, two main factors cause the difference between contactless and contact-based fingerprints. First, both are geometrically distorted, and there is a non-linear spatial transformation between them. Second, variation of the environmental conditions (*e.g.* different lighting situations) are more severe in capturing contactless samples. To address the perspective distortion problem, we develop a deep contactless fingerprint unwarping model in Section 2.1. In addition, we develop a model to extract ridge information of the unwarped samples in Section 2.2. At the end, we train the whole model concurrently by proposing a joint optimization process.

2.1. Contactless Fingerprint Unwarping Model

Given an input contactless sample x_p and the binarized ridge map of the equivalent contact-based fingerprint sample x_b, we seek to find the parameters Θ of a non-linear spatial transformation T such that unwarping x_p using $T(., \Theta)$ results in a unwarped sample x_u that has the maximum ridge overlap with x_b. The unwarped contactless sample can be formulated as:

$$x_u = T(x_p, \Theta). \tag{1}$$

To estimate the parameters of the warp, we use a non-linear function f which takes the input contactless sample x_p and estimates the set of parameters of warp $\Theta = f(x_p)$. We develop a CNN for the choice of f, and we train it using an end-to-end joint optimization which is discussed in Section 2.3. Having the estimator f, we can rewrite Equation 1 as:

$$x_u = T(x_p, f(x_p)). \tag{2}$$

Inspired by the previous approaches for rectifying distorted fingerprints [21, 22, 25, 7, 17], we define a statistical model to represent the perspective distortion of contactless fingerprints. We define a fixed regular sampling grid G_p on x_p which contains N horizontal and M vertical nodes. The corresponding grid G_u on the unwarped contactless sample is the result of transforming G_p using $T(., \Theta)$. Therefore, all the parameters of the warp can be obtained using these two grids. Instead of estimating the parameters of the warp directly, we estimate the displacement between the nodes of G_p and G_u. We develop two warp models to represent the displacements caused by the perspective distortion.

2.1.1 PCA-constrained Warp Model

A classical approach to model a warp [25] is to use a set of training samples representing the source and the target keypoints. We manually extract minutiae points from 400 contactless samples and their corresponding contact-based samples. We model the warp as a displacement of corresponding points on the original grid and the warped grid as follows:

$$d_i = v_i^u - v_i^p, \tag{3}$$

where d_i is the displacement field of minutia for the ith pair of contactless and its corresponding contact-based fingerprint, and v_i^u and v_i^P are the vectorized locations of all the points in grid G_u and G_p for the ith pairs of samples, respectively. Using PCA on the vectorized locations of all the training samples, we extract the principal components of the displacement between the two modalities [25, 7]. Approximation of the displacement fields using PCA is:

$$\hat{d} \approx \overline{d} + \sum_{i=1}^{t} c_i \sqrt{\lambda_i} e_i, \tag{4}$$

where $\overline{d}$ is the average displacement, t is the number of selected principal components for modeling the warp, c_i is the coefficient of the ith eigenvector component, e_i is ith eigenvector and λ_i is its corresponding eigenvalue. In this framework, the warp estimator f can estimate the warp by predicting the coefficients of the most significant principal components of the warp $\Theta^{PCA} = \{c_i : i \in \{1, .., t\}\}$ for an input contactless sample.

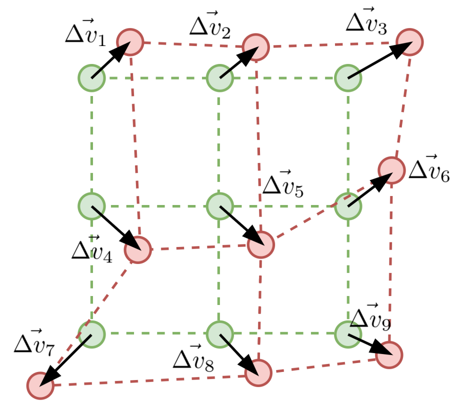

Figure 2. A sample demonstration of the free grid model of size 3×3. Green and red nodes denote the source and the target grid, respectively. In the free grid scenario for modeling the warp, the warp estimator estimates a displacement vector which consists of the differences between the locations of the source and target nodes.

2.1.2 Free Grid Warp Model

Modeling the statistics of the warp using PCA is highly dependent on the number of samples that are used for extracting the principal components of the warp. To have a more robust and flexible model for the warp, we develop a second warp model in which the warp parameters are directly defined as the displacement of each node in the target grid G_u

compared to G_p. Therefore, the target outputs of the warp estimator f for this model are expressed as $\Theta^{FG} = v_u - v_p$, where v_u and v_p are the vectorized locations of all points in grid G_u and G_p, respectively. Figure 2 shows a simple demonstration of the free grid method for modeling the warp.

So far, two warp models have been defined to represent the warp between the contactless and contact-based fingerprints. The parameters of the first warp are the coefficients of the PCA, and we refer to them as Θ^{PCA}. The parameters of the second warp are exactly the displacement of ridge information, and we refer to them as Θ^{FG}. Unfortunately, it is a difficult and labor-intensive task to extract minutiae from a contactless fingerprint (especially the marginal area of ridge information). Therefore, we do not have enough supervision (minutiae-annotated pairs of contactless and contact-based fingerprints) for training the deep CNN f. To overcome this issue, we develop a second model that indirectly provides the supervision needed to train the warp estimator model.

2.2. Ridge Enhancement Model

Given an unwarped contactless sample x_u, we develop a model to predict its ridge structure. For this purpose, one can adopt a classical ridge enhancement method, such as [11], which performs band-pass filtering for enhancing the ridge information. However, due to the lack of supervision for training the unwarping model, we seek to propose a joint optimization problem where the unwarping model can use the indirect supervision provided by the ridge enhancement unit through backpropagation. Therefore, we need to develop a differentiable ridge enhancement model so that the reconstruction loss can be used to update the parameters of the unwarping model. We adopt a deep U-Net model to predict the binarized ridge information of the unwarped contactless fingerprint. Given the unwarped sample x_u with a size of $w \times h$, the ridge enhancement model generates a binary map $y = G(x_u)$ of size $w \times h \times 2$ where $y^{(i,j,0)}$ and $y^{(i,j,1)}$ denote the predictions of the network as the probability of the pixel at the location (i, j) in x_u belonging to one of the classes of '*background*' or '*ridge*', respectively. In other words, this model is performing a dense binary classification for each pixel in the unwarped contactless fingerprint x_u.

2.3. End-to-end Joint Optimization

As discussed before, extracting minutiae from contactless fingerprints is a labor-intensive task, especially in the case of training a deep model where thousands of samples are needed for achieving reasonable performance. Without having the minutiae annotations, we do not have enough supervision for training the unwarping model. However, the contact-based equivalents of the contactless fingerprints are available, and we use them as the weak supervision for predicting the warp parameters. After enhancing the unwarped sample x_u, the final output of the model is a binarized ridge map as follows:

$$y = G\Big(T\big(x_p, f(x_p)\big)\Big). \tag{5}$$

Let y^* be the binarized ridge map of the contact-based fingerprint corresponding to the input sample x_p. We define the enhancement loss as the dense cross-entropy loss for all pixels in the output map as:

$$\mathcal{L}_{Enh} = \frac{-1}{wh} \sum_{i=0}^{w-1} \sum_{j=0}^{h-1} \sum_{k=0}^{1} y^{*(i,j,k)} \log y^{(i,j,k)}. \tag{6}$$

Due to the perspective distortion in contactless samples, ridge information in the center are clearer, and it is easier to reconstruct them. However, our goal is to unwarp and enhance the ridge information which is degraded due to the perspective distortion. Therefore, we develop a score map that shows which parts of the input sample contain more perspective distortion. We use this score map to force the network to pay more attention to distorted areas rather than clear ridges. The transformation T in Section 2.1 performs an spatial transformation using the parameters estimated by the unwarping model. During the unwarping process, T transforms each source location $u = (i, j)$ in the input contactless fingerprint to the target location $u' = (i', j')$ in the unwarped version. We use these source and target locations to estimate the amount of warp in each location of the input contactless fingerprint. We define a warp score map S as:

$$\begin{aligned} S = \{s_{i,j} = \sqrt{(i-i')^2 + (j-j')^2} \\ : \forall\, (i, j) \in \{1..w\} \times \{1...h\}\}, \end{aligned} \tag{7}$$

where $s_{i,j}$ shows the amount of warp at the location (i, j) in the input sample. We normalize S such that $s_{i,j} \in [\alpha, 1]$ as:

$$\hat{S} = \alpha + (1-\alpha)\frac{S - min\{S\}}{max\{S\} - min\{S\}}. \tag{8}$$

Finally, using this normalized score map $\hat{S}$, we rewrite Equation 6 as:

$$\begin{aligned} \mathcal{L}_{Enh} = \frac{-1}{wh \sum_{i=0}^{w-1} \sum_{j=0}^{h-1} \hat{s}_{i,j}} \times \\ \sum_{i=0}^{w-1} \sum_{j=0}^{h-1} \hat{s}_{i,j} \sum_{k=0}^{1} y^{*(i,j,k)} \log y^{(i,j,k)}. \end{aligned} \tag{9}$$

We use stochastic gradient descent to minimize $\mathcal{L}_{Enh}$. During the training, the error of the ridge segmentation

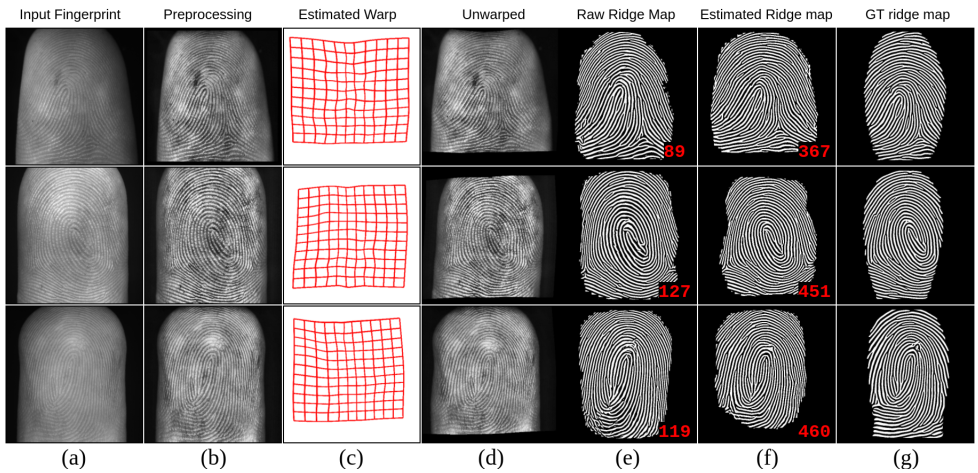

Figure 3. Examples of the processed samples using the proposed method. Columns from left to right: a) the input contactless fingerprints, b) the input samples after initial enhancement by adaptive histogram equalization, c) the deformation grid estimated using the final model (model D), d) unwarped contactless fingerprints, e) the ridge maps extracted directly from the unwarped samples using Gabor filtering, f) ridge maps estimated by the proposed ridge enhancer model, g) the ground truth ridge maps obtained from contact-based fingerprints. The red values show the VeriFinger [20] matching scores of the unwarped ridge maps against their corresponding ground truth ridge maps.

backpropagates to update the parameters of the ridge enhancer and the warp estimator network. It may be noted that the geometric transformer T is a differentiable TPS [10] which allows the gradients of the loss to be backpropagated to the warp estimator network. Therefore, the deep warp estimator updates its parameters without any direct knowledge about the ground truth parameters of the actual warp. Figure 1 shows the total structure of the proposed model.

2.4. Network Architecture

Our model consists of two deep CNNs. The first network acts as a non-linear regression model which estimates the continuous parameters of the warp. The number of outputs, N_o, of the warp estimator depends on the type of the warp model defined in Sections 2.1.1 and 2.1.2. For the case of the PCA-constrained model, we set $N_o = 4$, and the model estimates the coefficients for the top four significant eigen vectors of the warp. For the case of the free grid warp model, we set $N_o = 200$, and the model estimates the displacement of a grid with the size of 10×10 along two axes. Table 1 details the structure of the warp estimator and ridge enhancer networks.

3. Experiments

We define four test models to investigate the role of the warp models and the warp score map. Table 2 details these models. To evaluate the proposed method, we use two publicly available datasets of ManTech [9] and 2D/3D [28]. The ManTech dataset contains contactless and contact-based fingerprints from all fingers of 496 subjects. For each finger, 2 contactless fingerprints and several contact-based fingerprints captured using different sensors are available. We use all the 9,920 contactless samples and their corresponding contact-based samples for training our four models. The 2D/3D dataset has been published recently and contains 9,000 samples from 1,500 fingers. For each finger two contactless and 4 contact-based samples are available. We use samples from 500 fingers for fine-tuning the models trained on the ManTech dataset, and we use the rest of the dataset for testing the model.

We preprocess all the samples to reduce the variations of fingerprints. We first segment finger regions in all contactless samples by thresholding. Then we enhance the ridge information using adaptive histogram equalization. We fix and normalize the scale and rotation of samples using their median ridge frequency and orientation. For contact-based fingerprints, the median is computed over the whole area, and for contactless fingerprints, the median is computed over the central area of the fingerprint sample occupying 40 percent of the total ridge area. All samples are scaled to have a median ridge interval of 10 pixels. The final size of all samples is scaled to 256×256 which is the default spatial size of the input for our model.

We conduct several experiments to evaluate the proposed method using the experimental setup defined in [17] by generating $8,000$ $(1,000{\times}2{\times}4)$ genuine and $7,992,000$ $(1,000{\times}999{\times}4{\times}2)$ imposter pairs from the 2D/3D dataset. We compare our approach to several methods in the literature. In experiments 1 to 3, we match contactless and contact-based fingerprints directly without performing any unwarping process or enhancing using the NIST-NBIS [13], VeriFinger [20], and MCC [5] methods.

a) Warp Estimator			
# L	T	KS	OS
1	C,B,R,M	32	128, 32
2	C,B,R,M	64	64, 64
3	C,B,R,M	64	32, 64
4	C,B,R,M	128	16, 128
5	C,B,R,M	256	8, 256
6	C,B,R,M	512	4, 512
7	C,B,R,M	1024	2, 1024
8	C,B,R,M	2048	1, 2048
9	F,B,R	1024	1, 1024
10	F	1, N_o	1, N_o

b) Rige Enhancer										
#L	T	S	KS	OS	#L	T	S	KS	OS	Cn
1	V	1	64	256, 64	10	V	1	512	16, 512	-
2	V	2	128	128, 128	11	D	2	512	32, 512	L7
3	V	1	128	128, 128	12	V	1	512	32, 512	-
4	V	2	256	64, 256	13	D	2	256	64, 256	L5
5	V	1	256	64, 256	14	V	1	256	64, 256	-
6	V	2	512	32, 512	15	D	2	128	128, 128	L3
7	V	1	512	32, 512	16	V	1	128	128, 128	-
8	V	2	512	16, 512	17	D	2	64	256, 64	L1
9	V	1	512	16, 512	18	V	1	4	256, 2	-

Table 1. Architecture of a) warp estimator, and b) ridge enhancer. All layers of the warp estimator are formed by combining Convolution (C), Batch Normalization (B), ReLU (R), Max Pooling (M), and Fully-connected (F) modules. The spatial size of all kernels of the warp estimator are 3. The stride for all Convolutions are 1. N_o is the number of outputs described in Section 2.4. Each layer of the ridge enhancer is either a Convolution block V={C, B, R} or a Deconvolution block D={Transposed Convolution, B, R}. The number of kernels are denoted by 'KS', and the output size of each layer is denoted by 'OS'. Layers 1, 3, 5, and 7 of the ridge enhancer are concatenated to layers 17, 15, 13, and 11, respectively.

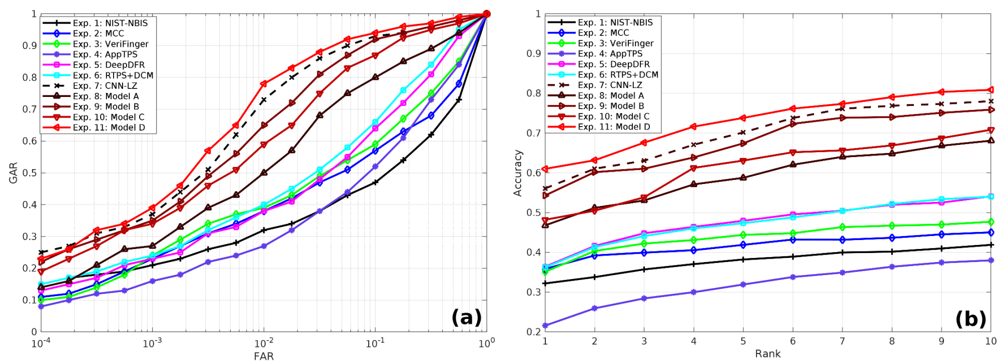

Figure 4. The a) ROC and b) CMC curves for the 11 cross-matching experiments. In experiments 1 to 3, the raw contactless samples are matched against the contact-based samples without any rectification. In experiments 4 to 6, contact-based fingerprints are rectified for elastic deformation before the matching. In experiment 7 samples are matched using a trained Simaese network [16]. Contrary to the previous methods, we first unwarp the contactless samples and then match them to contact-based fingerprints. Experiments 8 to 11 shows the performance of our four test models.

Test Model	A	B	C	D
Warp Model Sec. 2.1	PCA	FGrid	PCA	FGrid
Score Map Sec. 2.3	w/o	w/o	w/	w/

Table 2. Four test models defined in Sec. 3 to investigate the role of different warp models and the warp score map in the total performance of the model.

In experiments 4 to 7, we use the previously proposed methods of approximating TPS [2], deep fingerprint rectification [7], and robust TPS [17] to rectify contact-based fingerprints for elastic deformation and match them to contactless samples. It should be noted that contrary to the previous approaches [2, 25, 7, 17], we unwarp contactless fingerprints rather than rectifying contact-based fingerprints. In experiment 7 we implement a Siamese model to match contact-based fingerprints against the contactless samples as proposed in [16]. In the last four experiments, we match the unwarped and enhanced contactless fingerprints using the four variations of our model against contact-based fingerprints. We use the VeriFinger 7.0 standard SDK [20] as the matcher at the top of our algorithms.

For each experiment, we measure the performance of a method using Receiver Operating Characteristics (ROC) and Cumulative Matching Characteristic (CMC) curves which are plotted in Figure 4. Table 3 shows the equal error rate and Rank-1, Rank-5, and Rank-10 accuracy for all experiments. According to the experiments, we observe that the free grid warp model outperforms the PCA warp model developed for rectifying the elastic deformation of contact-based fingerprints [25]. On the other hand, we observe that the warp score map defined in Equation 7 significantly helps the ridge enhancement network to pay more attention to the unwarped areas, and as a result, indirectly provides more

Exp. #	Method	Equal Error Rate (%)	Rank-1 (%)	Rank-5 (%)	Rank-10 (%)
1	NIST-NBIS [13]	37.66	32.20	38.22	41.89
2	MCC [5]	32.10	35.84	41.90	45.03
3	VeriFinger [20]	25.32	35.13	44.40	47.70
4	Approximating TPS [2]	26.83	21.59	31.93	38.00
5	DeepDFR [7]	21.34	36.41	47.95	53.11
6	RTPS+DCM [17]	19.81	36.25	47.34	54.01
7	CNN-LZ [16]	8.38	56.08	70.17	78.04
8	Model A: PCA w/o ScoreMap	16.25	46.80	58.76	68.10
9	Model B: FGrid w/o ScoreMap	8.90	54.32	67.43	75.90
10	Model C: PCA w/ ScoreMap	11.16	48.20	63.09	70.84
11	Model D: FGrid w/ ScoreMap	**7.71**	**61.01**	**73.82**	**80.88**

Table 3. Detailed comparison of EER, Rank-1, Rank-5, and Rank-10 of cross-matching results on the 2D/3D dataset.

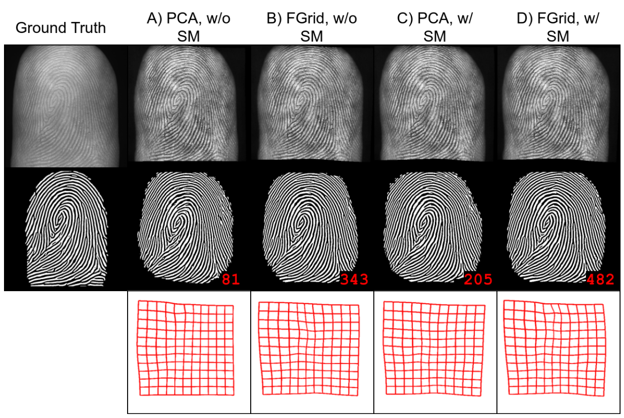

Figure 5. Comparison of the outputs of the four models described in Sec. 3. The top row shows the ground truth contactless fingerprint and its unwarped versions. The middle row shows the ground truth ridge map and the final outputs of the four models. The red score shows the matching score between the ridge map and the ground truth obtained using VeriFinger [20]. The bottom row shows the estimated warps for each model.

robust supervision for the warp estimator network. Figure 5 provides a visual comparison of the results obtained from all four test models. We select model 'D', which utilizes the free grid warp model and the warp score map, as the superior model of this study due to its significant performance compared to other three models. Figure 3 shows some examples processed by this model. In another experiment, we measure the number of minutiae detected by the NIST-NBIS [13] and VeriFinger [20]. Table 4 shows the number of minutiae extracted from the unwarped contactless fingerprints. This shows that unwarping the contactless fingerprint can reveal some valuable information from the distorted part of the sample. More specifically, samples unwarped by our final model contain approximately 17% more minutiae compared to the original contactless fingerprints.

	NBIS	VeriFinger
Original	36.74	38.20
Unwarped-Model A	40.85	41.04
Unwarped-Model B	42.43	43.22
Unwarped-Model C	41.54	42.37
Unwarped-Model D	**43.81**	**44.58**

Table 4. Average number of minutiae extracted from contactless fingerprints before and after the unwarping process. Unwarping samples by model 'D' results in approximately 17% more minutiae compared to the original contactless samples.

4. Conclusion

In this study, we proposed to unwarp the contactless fingerprints to reduce the spatial mismatch introduced by the perspective distortion and recover information from severely distorted parts of the contactless samples. A critical issue faced when rectifying the perspective distortion is the lack of enough minutia-annotated pairs of contactless and the corresponding contact-based fingerprints. To overcome this hurdle, we proposed a deep contactless fingerprint unwarping model which indirectly learns to unwarp contactless fingerprints without having any supervision for the desired warp parameters. The warp estimator model learns to unwarp the input contactless fingerprint such that the unwarp sample has enough overlap with its corresponding contact-based fingerprint. The overlapping information of the unwarped contactless fingerprint is computed by the second model, a differentiable ridge enhancer, and the error of alignment is used to update the parameters of both models simultaneously. The performance of the proposed model is evaluated on two public datasets of contactless fingerprints and is compared to several state-of-the-art methods for rectifying fingerprint distortion. Extensive experiments showed that, on average, the proposed model can recover 17% more minutiae from the contactless fingerprints compared to the raw samples.

References

[1] G. Abramovich, K. Harding, S. Manickam, J. Czechowski, V. Paruchuru, R. Tait, C. Nafis, and A. Vemury. Mobile, contactless, single-shot, fingerprint capture system. In *Biometric Technology for Human Identification VII*, volume 7667, page 766708. International Society for Optics and Photonics, 2010.

[2] A. M. Bazen and S. H. Gerez. Fingerprint matching by thin-plate spline modelling of elastic deformations. *Pattern Recognition*, 36(8):1859–1867, 2003.

[3] F. L. Bookstein. Principal warps: Thin-plate splines and the decomposition of deformations. *IEEE Transactions on pattern analysis and machine intelligence*, 11(6):567–585, 1989.

[4] K. Cao and A. K. Jain. Latent fingerprint recognition: Role of texture template. *arXiv preprint arXiv:1804.10337*, 2018.

[5] R. Cappelli, M. Ferrara, and D. Maltoni. Minutia cylinder-code: A new representation and matching technique for fingerprint recognition. *IEEE Transactions on Pattern Analysis and Machine Intelligence*, 32(12):2128–2141, 2010.

[6] Y. Chen and A. K. Jain. Dots and incipients: extended features for partial fingerprint matching. In *Biometrics Symposium 2007*, pages 54–59, 2007.

[7] A. Dabouei, H. Kazemi, S. Iranmanesh, J. Dawson, and N. Nasrabadi. Fingerprint distortion rectification using deep convolutional neural networks. In *The 11th IAPR International Conference on Biometrics (ICB 2018)*, 2018.

[8] A. Dabouei, S. Soleymani, H. Kazemi, S. M. Iranmanesh, J. Dawson, and N. M. Nasrabadi. ID preserving generative adversarial network for partial latent fingerprint reconstruction. *arXiv preprint arXiv:1808.00035*, 2018.

[9] L. Ericson and S. Shine. Evaluation of contactless versus contact fingerprint data phase 2 (version 1.1). *DOJ Office Justice Programs, I. ManTech Adv. Syst. Int., Fairmont, WV, USA, Tech. Rep*, 249552, 2015.

[10] M. Jaderberg, K. Simonyan, A. Zisserman, et al. Spatial transformer networks. In *Advances in neural information processing systems*, pages 2017–2025, 2015.

[11] A. Jain and L. Hong. On-line fingerprint verification. In *Pattern Recognition, 1996., Proceedings of the 13th International Conference on*, volume 3, pages 596–600. IEEE, 1996.

[12] T.-Y. Jea and V. Govindaraju. A minutia-based partial fingerprint recognition system. *Pattern Recognition*, 38(10):1672–1684, 2005.

[13] K. Ko. User's guide to NIST biometric image software (NBIS). Technical report, 2007.

[14] A. Kumar and Y. Zhou. Contactless fingerprint identification using level zero features. In *Computer Vision and Pattern Recognition Workshops (CVPRW), 2011 IEEE Computer Society Conference on*, pages 114–119. IEEE, 2011.

[15] R. D. Labati, A. Genovese, V. Piuri, and F. Scotti. Contactless fingerprint recognition: a neural approach for perspective and rotation effects reduction. In *Computational Intelligence in Biometrics and Identity Management (CIBIM), 2013 IEEE Workshop on*, pages 22–30. IEEE, 2013.

[16] C. Lin and A. Kumar. Multi-siamese networks to accurately match contactless to contact-based fingerprint images. In *Biometrics (IJCB), 2017 IEEE International Joint Conference on*, pages 277–285. IEEE, 2017.

[17] C. Lin and A. Kumar. Matching contactless and contact-based conventional fingerprint images for biometrics identification. *IEEE Transactions on Image Processing*, 27(4):2008–2021, 2018.

[18] C. Lin and A. Kumar. A CNN-based framework for comparison of contactless to contact-based fingerprints. *IEEE Transactions on Information Forensics and Security*, 14(3):662–676, 2019.

[19] X. Liu, M. Pedersen, C. Charrier, F. A. Cheikh, and P. Bours. An improved 3-step contactless fingerprint image enhancement approach for minutiae detection. In *Visual Information Processing (EUVIP), 2016 6th European Workshop on*, pages 1–6. IEEE, 2016.

[20] Neurotechnology Inc., Verifinger. http://www.neurotechnology.com.

[21] A. Ross, S. Dass, and A. Jain. A deformable model for fingerprint matching. *Pattern Recognition*, 38(1):95–103, 2005.

[22] A. Ross, S. C. Dass, and A. K. Jain. Fingerprint warping using ridge curve correspondences. *IEEE Transactions on Pattern Analysis and Machine Intelligence*, 28(1):19–30, 2006.

[23] A. Sankaran, A. Malhotra, A. Mittal, M. Vatsa, and R. Singh. On smartphone camera based fingerphoto authentication. In *Biometrics Theory, Applications and Systems (BTAS), 2015 IEEE 7th International Conference on*, pages 1–7. IEEE, 2015.

[24] A. W. Senior and R. M. Bolle. Improved fingerprint matching by distortion removal. *IEICE Transactions on Information and Systems*, 84(7):825–832, 2001.

[25] X. Si, J. Feng, J. Zhou, and Y. Luo. Detection and rectification of distorted fingerprints. *IEEE transactions on pattern analysis and machine intelligence*, 37(3):555–568, 2015.

[26] C. Stein, C. Nickel, and C. Busch. Fingerphoto recognition with smartphone cameras. In *Biometrics Special Interest Group (BIOSIG), 2012 BIOSIG-Proceedings of the International Conference of the*, pages 1–12. IEEE, 2012.

[27] K. Tiwari and P. Gupta. A touch-less fingerphoto recognition system for mobile hand-held devices. In *Biometrics (ICB), 2015 International Conference on*, pages 151–156. IEEE, 2015.

[28] W. Zhou, J. Hu, I. Petersen, S. Wang, and M. Bennamoun. A benchmark 3D fingerprint database. In *Fuzzy Systems and Knowledge Discovery (FSKD), 2014 11th International Conference on*, pages 935–940. IEEE, 2014.